

CH Cyg X-ray Jet Activity and Multi-component Structures

Margarita Karovska¹

Christopher L. Carilli²

John C. Raymond¹

Janet A. Mattei³

ABSTRACT

In this paper we report detection of multiple component structures in a Chandra X-ray image obtained in March 2001 of the nearby symbiotic interacting binary system CH Cyg. These components include a compact central source, an arc-like structure or a loop extending to $1.5''$ (400 AU) from the central source associated with the 1997 jet activity, and possibly a newly formed jet extending to ~ 150 AU from the central source. The structures are also visible in VLA and HST images obtained close in time to the Chandra observations. The emission from the loop is consistent with optically thin thermal X-ray emission originating from a shock resulting from interaction of the jet ejecta with the dense circumbinary material. The emission from the central source originates within < 50 AU region, and is likely associated with the accretion disk around the white dwarf. CH Cyg is only the second symbiotic system with jet activity detected at X-ray wavelengths, and the Chandra high-angular resolution image, combined with the VLA and HST images, provides the closest view of the region of jet formation and interaction with the circumbinary material in a symbiotic binary.

Subject headings: accretion, accretion disks — binaries: close — stars: individual (CH Cyg) — binaries: symbiotic, stars: winds, outflows — x-rays: general

¹Smithsonian Astrophysical Observatory, 60 Garden St., Cambridge, MA 02138; mkarovska@cfa.harvard.edu.

²National Radio Astronomy Observatory, PO Box O, Socorro, NM 87801

³American Association of Variable Star Observers, 25 Birch Street, Cambridge, MA 02138

1. INTRODUCTION

Symbiotic systems are interacting binaries showing a composite spectrum with signatures of a late-type giant and a high-temperature component, often a compact accreting object. As with many other astronomical sources, accretion is thought to be the primary energy source in these systems. The interaction between the components occurs via wind accretion and/or Roche lobe overflow. Symbiotic systems are a very important subgroup of interacting binaries because they are among the likely candidates for progenitors of bipolar planetary nebulae, and they have also been invoked as potential progenitors of at least a fraction of Supernovae type Ia, key cosmological distance indicators (e.g. Chugai and Yungelson 2004). So far there are only a couple hundred known members in this class.

CH Cyg is one of few symbiotic systems showing jet activity (e.g. Corradi *et al.* 2001, Kellogg *et al.* 2001). At a distance of 245^{+50} pc (Perryman *et al.* 1997) CH Cyg is one of the closest symbiotic systems, therefore providing a unique opportunity for high-angular resolution imaging of a close circumbinary environment in an interacting binary, including the region of jet formation and early propagation.

The CH Cyg system is composed of an evolved M6-7 III giant and an accreting white dwarf. There is also evidence for a third body in the system, also an evolved giant (e.g. Hinkle *et al.* 1993, Scopal *et al.* 2002). This binary is one of the most fascinating objects in its class because of its extremely complex circumbinary environment, and its dramatic outbursts.

In the past few decades CH Cyg has undergone several outbursts, each preceded by extended intervals of quiescence (Karovska and Mattei 1992, Sokoloski and Kenyon 2003, Eyres *et al.* 2002, Skopal *et al.* 2002). Since 1984, when a powerful jet was formed in the midst of a prominent radio and optical outburst (Taylor *et al.* 1986), several outbursts have been detected including in 1996 and in 1998 (Karovska *et al.* 1998a&b, Eyres *et al.* 2002). Radio monitoring of the system has shown indications of a possible precessing jet with enhanced activity associated with occasional outbursts (Crocker *et al.* 2002).

Observations of CH Cyg have been carried out over the past two decades using several X-ray satellites. Spectral modeling indicates a multi-component structure in the emission from this system (Leahy and Taylor 1987; Leahy and Volk 1995; Ezuka *et al.* 1998; Mukai *et al.* 2006). For example, Ezuka *et al.* (1998) detected a soft component in the ASCA spectrum with flux of 3.7×10^{-12} *ergs cm⁻²s⁻¹* from 0.5 to 2.5 keV. They modeled this emission as two optically thin thermal plasma emissions, the temperatures of which are 0.2 and 0.7 keV. However, the origin of the soft component remained unclear. A previously unknown hard component was also detected in the spectrum with flux of 6.9×10^{-12} *ergs cm⁻²s⁻¹*

in the region from 2-10 keV. This component was modeled with optically thin thermal plasma emission with temperature of 7.3 keV, undergoing a strong photoelectric absorption with $N_H = \sim 10^{23} \text{ cm}^{-2}$. In addition, several emission features were detected including iron emission lines between 6 and 7 keV. Wheatley and Kallman (2006) re-analyzed the ASCA spectrum and concluded that there is only one emission component. They suggest that similar to Seyfert 2 galaxies, the soft emission is due to scattering of the hard component in a photoionized medium surrounding the white dwarf. Mukai *et al.* (2006) analyzed recent Suzaku observations and found that the large equivalent width of the 6.4 keV fluorescence line implies that the hard X-rays are indeed dominated by scattering. However, they concluded that there are two distinct components responsible for the hard and soft X-ray emission. They also confirmed that there is a significant long-term variability in the X-ray emission in the system.

Chandra observations carried out in 2001 detected an elongation in the CH Cyg image, extending 2-4" to the south from the central source. Galloway and Sokoloski (2004) attributed this extension to jet activity associated with the white dwarf. This is only the second source from a population of few hundred known symbiotics showing jet activity in X-rays. However, in the Galloway and Sokoloski (2004) analysis of the Chandra image the potential spatial resolution of $<0.5''$ on-axis was significantly degraded by gaussian smoothing used to enhance the faint extended emission. Therefore, the resolution was insufficient to study directly the spatial distribution of the X-ray emission.

In this paper we present results from our further detailed spatial analysis of the Chandra observation of CH Cyg combined with the results from VLA and HST imaging of the system. Using the full angular resolution potential of Chandra we identify several distinct spatial components contributing to the X-ray emission and resolve the ambiguity left from previous X-ray observations regarding the extended emission and the contributors to the soft and the hard component of the X-ray spectrum of CH Cyg.

2. CHANDRA OBSERVATIONS AND ANALYSIS

The Chandra pointed observations of CH Cyg were carried out over 47 ks on 2001 March 27 (OBSID 1904) using the ACIS-S instrument in combination with HETG grating (Weisskopf *et al.* 2002). Significant signal was detected mostly in the zeroth-order of the spectrum; a total of 770 counts were detected from 0.2 to 8 keV. We analyzed the *Chandra* observations using *CIAO* data reduction and analysis routines. In our analyses we used *Ciao* 3 and cal database 2.2 (similar to Galloway and Sokoloski 2004), as well as the more recent

Ciao 3.3 version.¹

Chandra data include information about the photon energies and positions. This information was used to obtain energy-filtered images and to carry out sub-pixel resolution spatial analysis (*vis* Karovska *et al.* 2005). Based on the three spectral emission components identified by Ezuka *et al.* (1998) and Galloway and Sokoloski (2004) (see for example Fig. 3 in Galloway and Sokoloski 2004) we created images in the soft band (0.2-2keV), the hard band (2-6 keV), and in the spectral region around the strong emission feature at 6.5-7 attributed to 6.67 keV iron line. The total counts detected in these images using a circular region with a radius of 5" centered on the brightest central source are: 290, 260, and 100 counts, respectively. The expected X-ray background in the region is negligible.

We explored the spatial distribution of the emission in the images of the system at 0.2" resolution using deconvolution and smoothing techniques. The pixel size of the *Chandra*/ACIS detector is 0.492". However, due to the telescope dither smaller spatial scales are accessible as the image moves across the detector pixels. This sampling of smaller than detector pixel scales allows sub-pixel analysis and deconvolution. Similar techniques were applied for resolving Mira AB 0.5" binary system (Karovska *et al.* 2005), as well as for SN1987A (e.g. Burrows *et al.* 2000, Park *et al.* 2002) which allowed resolving sub-arcsecond structures in the 1" scale SN remnant. After processing of the data (including with pixel randomization turned off) we binned the images with 0.1" pixels.

We used PSF simulations for comparison with the observations in order to evaluate detected structures in the observed images as well as to estimate the extent of the central source in different spectral bands. The PSF simulations were carried out using information on the spectral distribution and off-axis location of the system as inputs to ChaRT PSF simulator² (Karovska *et al.* 2003).

To detect the low contrast diffuse emission we applied the adaptive smoothing CIAO tool *csmooth*, based on the algorithm developed by Ebeling *et al.* (2006) and implemented in *asmooth*. *Csmooth* is an adaptive smoothing tool for images containing multiscale complex structures, and it preserves the spatial signatures and the associated counts as well as significance estimates. The smoothing is achieved by convolution with a gaussian kernel. The size of the kernel increases from a small initial value and the smoothing scale is increased until the total number of counts under the kernel exceeds a value that is determined from a preset

¹CIAO is the Chandra Interactive Analysis of Observation's data analyses system package (<http://cxc.harvard.edu/ciao>)

²<http://asc.harvard.edu/chart/index.html>

significance and the expected number of background counts in the kernel area. Significance is computed at each pixel location for each smoothing scale by comparing the total counts under the kernel to the background in the same area. Pixels for which the significance exceeds the threshold value set by the user are smoothed at the current scale, and are excluded from subsequent smoothing steps at larger scales.

In Figure 1 we display the smoothed images of CH Cyg in the soft (0.2-2), and the hard (2-6 keV) bands. In these images we show structures smoothed above 3σ significance level, and the smoothing scales vary from 0.2 to 0.5 arcseconds. A compact central source is detected in all three bands. Our analysis shows that the central sources in the hard band image and in the 6.5 to 7 keV image are consistent with unresolved point sources (FWHM less than $0.2''$). In addition to a central source, several extended structures are detected that are especially prominent in the soft image. For the central source, within a circular region with $0.3''$ radius, we estimate a hardness ratio of ~ 2 , (counts $>2\text{keV}$ divided by the counts $< 2\text{ keV}$).

Figure 2 shows the smoothed soft image, as in Figure 1, with overplotted contours of the simulated Chandra PSF. When compared to the PSF this image shows a somewhat extended central source to $\sim 0.7''$ at P.A. $\sim 150/330$ degrees, and an extended emission to the south consisting of at least two components: a loop-like structure, and a faint emission extending beyond the loop. Figure 3 displays the soft image after subtracting the PSF, showing the extended structure in the central source at P.A. ~ 330 degrees and the loop-like structure to the south.

The loop-like structure extends to a distance of $\sim 1.5''$ from the central source. The southern part of the loop appears brighter and resembles an arc. There are regions of enhanced brightness ($3-5\sigma$) in the southern portion of this loop, smoothed on scales of 0.3 arcseconds. We detect ~ 40 counts in the region of the loop structure. The emission in the loop region is fainter in the images above 2keV and contains about half of the counts in the soft image. The low counts are insufficient to extract detailed spectral information; however, the loop clearly shows a soft X-ray signature. There is also a faint emission beyond the loop extending to $\sim 4''$ south of the central source. This feature could be associated with a diffuse emission with a low surface brightness (total ~ 20 counts).

The multi-component structure in CH Cyg was not detected in the Galloway and Sokoloski (2004) image because they applied gaussian smoothing with a FWHM of $2''$ which resulted in degraded resolution. In Figure 4 we compare our soft band high-angular resolution image with their result. Although they did detect an extension of a few arcseconds from the central source, their smoothed image did not permit detection of the multi-component structures, including the loop-like structure separated from the central source, which are

clearly seen in our adaptively smoothed images.

We further explored the reality of these low-count structures by applying a statistical deconvolution technique EMC2 (Expectation through Markov Chain Monte Carlo) specifically applicable to low-counts Poisson data (Esch *et al.* 2004). This technique uses a wavelet-like multiscale representation of the true image in order to achieve smoothing at all scales of resolution simultaneously. Wavelet decomposition of the image allows the Poisson likelihood to be factored into separate parts, corresponding to the wavelet basis. Each of these factors in the likelihood can be reparametrized as a split of the intensity from the previous, coarser factor. A *prior* is assigned to these splits (which can be viewed as smoothing parameters), and then a model is fit using Markov Chain Monte Carlo (MCMC) methods. In this way small and large-scale structures in the image are captured, e.g. diffuse emission as well as point sources and sharp features in the image. This Bayesian model-based analysis allows assessment of the uncertainties in the reconstructed image. Details of this technique and examples are described in Esch *et al.* 2004. The EMC2 has been applied to various data sets including to Chandra observations (e.g. Esch *et al.* 2004, Karovska *et al.* 2005).

We used EMC2 and the simulated PSF to perform deconvolution of the CH Cyg soft X-ray image. Figure 5 displays the EMC2 deconvolved image showing complex multi-component structures with significance above 3σ . The structures are similar to those resulting from adaptive smoothing, but with improved resolution. In addition to the loop-like structure to the south of the central source, the central source appears to have a compact core and an elongated structure extending to $\sim 0.7''$ at the P.A. of 330 deg. A fainter structure is seen to the south at about same distance from the source at P.A. of 150 deg.

The structures detected in the X-ray images of CH Cyg are very similar to the structures detected in radio and optical observations obtained close in time to the Chandra observations as described in the following section.

3. COMPARISON WITH HST AND VLA OBSERVATIONS

Optical/UV and radio images of CH Cyg obtained since 1996 show a complex circumbinary environment including ionized outflow, and structures associated with jet or outburst activity in the system (e.g. Corradi *et al.* 2001; Eyres *et al.* 2002).

Although there are no observations contemporaneous with the 2001 Chandra observation, we identified a set of VLA and HST observations that were carried out close in time to the Chandra observations. Radio maps of CH Cyg were obtained using the VLA at 5GHz and 8GHz on 2000 November 9 about 4.5 months before the Chandra observation. HST

observations were carried out on 1999 August 13 (in the optical, with WFPC2), 1.6 years before the Chandra observations.

The loops detected in the soft X-ray image are similar to the arc-like extensions observed in the HST WFPC2 images (Eyres *et al.* 2002, and Crocker *et al.* 2002). The HST/WFPC2 images obtained 1.6 years before the Chandra observations are dominated by the UV continuum, [OIII], H α and H β lines. They show extended emission to the north and to the south of the central region. Several structures, including an arc-like structure 1.2" to the south of the central source, have been detected in this extended emission (e.g. Eyres *et al.* 2002). The loop-like structure is most clearly visible in the 502N [OIII] image.

In Figure 5 we compare the deconvolved Chandra soft X-ray image with the HST [OIII] image which has a similar resolution.

We note that the HST observation is the same as shown in Figure 1 in Galloway and Sokoloski (2004). The extended [OIII] structures show three distinct components: a central source, $\sim 0.5''$ extensions to the north well as at \sim PA160 deg to the south, and a loop-like feature to the south at 1.2". The [OIII] loop-like feature fits within the loop in the Chandra soft image, as shown in Figure 5. The south side of the [OIII] loop appears brighter as seen in the X-ray image.

The VLA map shown in Figure 6 was made from data taken on November 9, 2000 (VLA in the "A" configuration). The resolution is $0.55'' \times 0.39''$ with major axis position angle = -82° , and the rms = $35 \mu\text{Jy beam}^{-1}$. This map shows a very similar morphology when compared to the soft band Chandra image; it shows a central structure extended at P.A. \sim 330 degrees, as well a loop like structure $\sim 1.5''$ to the south. The total flux density from the source is 7.2 mJy, with a peak surface brightness of $2.4 \text{ mJy beam}^{-1}$ at $19^h 24^m 33.03^s +50^\circ 14' 27.1''$ (J2000). The loop structure shows enhancement in the south side, similar to that of the X-ray loop. The southern loop has an integrated radio flux of 1.6 mJy. The core source has an inverted spectrum of index $\alpha = +0.6$, between 5 and 8 GHz, suggesting optically thick emission. We define α as $S_\nu \propto \nu^\alpha$. The northern extension has flat spectrum, $\alpha \sim 0$, suggesting optically thin free-free emission. The southern loop has a steep spectrum, $\alpha \sim -0.8$, implying optically thin non-thermal emission. The minimum energy magnetic field in the southern loop based on the non-thermal radio surface brightness is about 1mG, with a minimum pressure of $6 \times 10^{-8} \text{ dynes cm}^{-2}$.

In Figure 6 we display an overlay of the radio contours on the smoothed soft X-ray image, which has a similar resolution. The radio and the X-ray loops are cospatial within the resolution limit of the VLA data of $\sim 0.4''$. We note that the resolution in the X-ray and radio images is insufficient to determine if the regions of X-ray and radio emission are

separated.

4. DISCUSSION

Our analysis of the Chandra data shows that there are several spatially distinct X-ray emission components in the CH Cyg system. The X-ray emission in the CH Cyg image is dominated by an unresolved central core, however, there are several extended components that contribute as well. The emission from the central core originates within a region of less than 50 AU, which is only few times larger than the binary separation. This is as close as we can get to the central region of an interacting binary with today's X-ray imaging capabilities.

The hard emission from the central core, including in the iron line, probably originates in the inner region of the accretion disk or in a boundary layer between the accretion disk and the white dwarf. The soft emission from the unresolved core may be attributed to the accretion disk itself or to scattered hard X-rays from the inner disk region by the outer disk or corona. The scattering could be due to a non isotropically distributed ionized photoionized medium similar to Seyfert 2 galaxies (e.g. Wheatley and Kallman 2006). The X-ray emission in CH Cyg core appears harder than in other symbiotics, eg. in R Aqr and Mira AB (Kellogg et al 2001, Karovska et al 2005), which have relatively soft spectra, close to 1 keV. Geometry of the surrounding material may play a role since part of the hard X-rays in these systems may be absorbed or scattered in a different way.

In addition to the unresolved core, the soft X-ray image shows a second component in the central region, an extended structure to ~ 150 AU at 330/150 degrees. This structure was also detected in the radio, and HST O[III] images. The emission could be due to a shocked gas formed in the region of collision between the fast wind from a white dwarf with the red giant wind. However, since the orientation of this structure is similar to that of radio and optical jets observed in the past, and to the general orientation of the loop structures further to the south (e.g. Eyres *et al.* 2002, Corradi *et al.* 2001), we believe that the structure is more likely associated with a recent jet activity, e.g., during the 1998-2000 active phase. The emission could result from jet interaction with the close circumbinary material including circumstellar dust shells surrounding the giant. In fact, Mid-IR photometry does show the presence of a significant dust in the vicinity of the central region of CH Cyg (Teranova and Shenavrin 2004). Furthermore, high-angular resolution Mid-IR imaging of CH Cyg detected a dusty circumstellar feature $\sim 0.7''$ to the North of central source, similar to the extension of the feature detected in Chandra, Radio and HST images (Biller *et al.* 2006). Follow up observations of this extended X-ray structure are needed to determine its nature and kinematics.

Our imaging shows that although the X-ray emission from the central region dominates the soft emission in CH Cyg, a significant fraction ($\sim 20\%$) originates further away, from the loop at ~ 400 AU and from the extended diffuse emission beyond. The loop is likely associated with the 1997 radio outburst which was followed by jet activity (Karovska *et al.* 1998a, Karovska *et al.* 1998b). The 1997 radio outburst in CH Cyg was detected using the VLA at several frequencies (Karovska *et al.* 1998a). Nearly contemporaneous continuum measurements at millimeter and submillimeter wavelengths with the IRAM interferometer and with SCUBA on the James Clerk Maxwell Telescope also showed evidence for a strong radio outburst (Mikolajewska *et al.* 1998). The 1997 radio outburst occurred following an unprecedented drop in the V magnitude in 1996 (Karovska *et al.* 1998a), similar to a previous event in 1984, following which a powerful jet was formed (Taylor *et al.* 1986). In early 1998 we detected a radio jet using the VLA in its highest resolution observing mode (Karovska *et al.* 1998b). At that time, the radio maps detected two structures with a roughly North-South orientation, with the southern structure separated from the central source by about $0.35''$. The VLA observations of the loop carried out later on in 2000 show that the structure has expanded to a distance close to $1.5''$, or ~ 375 AU. This corresponds to an expansion velocity of ~ 400 km/s.

Assuming that the loops we detected in the X-rays and radio, and in [OIII], are a consequence of the same outburst event, the [OIII] loop would have had to expand at a velocity of several hundred km/s to reach the position seen in the Chandra images 1.6 years later. It would also have taken a few years for ejecta from the central region with an expansion velocity of few hundred km/s to reach the apex of the [OIII] loop, and then to expand to the region of the radio and X-ray loops (assuming that the ejecta have not been slowed down since the outburst). This is in agreement with the apparent expansion velocity derived from the 1998 VLA observations.

Kinematic studies of outflows in CH Cyg do show velocities of the expanding material on the order of few hundred km/s (Corradi *et al.* 2001) which is in agreement with the velocity of expansion that we calculated. On the other hand, spectroscopic observations also show evidence for mass ejections in CH Cyg that indicate much higher velocities, well over 1000 km/s (e.g. Skopal *et al.* 2002). Skopal *et al.* (2002) suggested that this difference could be due to a significant deceleration of the ejecta due to interaction with the circumstellar medium, which would be also in agreement with our observations. On the other hand, if the ejecta have not been slowed down and are moving with a speed over 1000 km/s, there remains a possibility that the X-ray and radio emission in the region of the loop may be a consequence of an outburst during the more recent 1998-2000 active phase.

The X-ray emission from the loop is consistent with a shock generated by ejecta colliding

with the surrounding pre-existing circumstellar material. The X-ray emission beyond the loop could be associated with continuous interaction of the expanding wind with the pre-existing circumbinary material, or it could result from more intermittent shocks associated with a pulsed jet (e.g., Stute 2006). The non-thermal spectral index of the radio emission could be explained by particle acceleration at the shock.

The small number of counts in the loop do not permit us to fit for the temperature and absorbing column of the emitting gas. If we make the most favorable assumptions given the 60 counts detected and the hardness ratio, the temperature is about 1 keV and the luminosity is about 5×10^{28} erg s⁻¹. For a 400 AU sphere and an X-ray emissivity of 2×10^{-23} erg cm³ s⁻¹ (e.g. Raymond, Cox & Smith 1976), the density is about 50 cm⁻³. This estimate is probably on the low side, given that the spherical volume is not filled and that absorption will reduce the observed count rate. Nevertheless, it implies a pressure about 2.5 times the minimum magnetic pressure estimated from the radio emission. The mass of the X-ray emitting gas is about 10²⁶ g, or 0.1, 0.05 and 1.0 times the masses of jet components A, B and C measured by Taylor et al. (1986), respectively. Given that the velocity ellipses measured by Corradi et al. (2001) suggest shock speeds of about 100 km/s, while the X-rays require shock speeds near 1000 km/s, the simplest interpretation is that the jet is underdense by a factor of 100 compared to the ambient gas. The slower shock in the ambient gas produces Balmer line, [O II] and [O III] emission by a combination of shock heating and photoionization of the compressed gas. Because the gas cools quickly the compression is very strong. The fast shock produces X-rays, but a shock speed closer to 2000 km s⁻¹ than 1000 km s⁻¹ may be required, since electron temperatures are generally well below proton temperatures in such fast shocks (e.g. Rakowski 2006). The radio emission could come from either shock, but the strong magnetic field suggests that it originates in gas that has been strongly compressed by the slower shock. If the first shock generates the radio emission, a significant magnetic field, on the order of 25 μG, would be required in the jet.

A high speed (precessing) jet may also clear a cavity in the pre-existing circumstellar material (e.g. Ybarra *et al.* 2006). The X-ray and the radio emission in that case originate from a loop-like structure delineating a shock region in the boundary between the walls of the cavity and the surrounding material. A similar scenario has been suggested for the loop-like structure observed previously further away ($\sim 5''$) from the central source in the UV O[II] HST images of CH Cyg (Corradi *et al.* 2001).

5. CONCLUSIONS

Our study of the CH Cyg close circumbinary environment using a combination of multi-wavelength X-ray, radio and optical high-angular resolution observations identified several distinct components in this system. These include a compact central source, and several extended structures likely associated with jet activity. These results are important since CH Cyg is only the second symbiotic system after R Aqr (Kellogg *et al.* 2001) with jet activity detected at X-ray wavelengths, and the Chandra image combined with the VLA and HST data provides the closest view of the region where jets are being formed and interacting with the surrounding material as they propagate through the circumbinary environment. Furthermore, our analysis of the Chandra data resolves the ambiguity as to whether there is only one (Wheatley and Kallman 2006), or multiple components (e.g. Ezuka *et al.* 1998, Mukai *et al.* 2006) contributing to the X-ray emission from this system.

Continuing multiwavelength monitoring of CH Cyg is necessary to determine the characteristics of the multi-component structures and their evolution as they interact with the surrounding circumbinary environment. It is especially important to obtain longer exposure X-ray observations of this system which will increase the signal-to-noise in the images and allow deriving spectral characteristics of the emissions from individual components.

Janet Mattei passed away before the completion of this article, and her coauthors respectfully dedicate it to her memory. We are grateful to W. Hack for providing the drizzled HST image of CH Cyg, and to AAVSO for providing the CH Cyg light curve. We thank Y. Butt for useful discussions. We would like to thank the anonymous referee for helpful comments and suggestions. MK is a member of the Chandra X-ray Center, which is operated by the Smithsonian Astrophysical Observatory under NASA Contract NAS8-03060. CC would like to acknowledge support from the Max-Planck Society and the Alexander von Humboldt Foundation through the Max-Planck-Forschungspreis 2005.

REFERENCES

- Biller *et al.* 2006, astro-ph 0604336
Burrows, D.N. *et al.* 2000, ApJ, 543,149
Chugai, N.N., and Yungelson, L.R., 2004, Astron. Lett., 30, 65.
Corradi R.L.M. et al., 2001, ApJ, 560, 912.

- Crocker, M.M., Davis, R.J., Spencer, R.E., Eyres, S.P.S., Bode, M.F., Skopal, A., 2002, MNRAS, 335, 1100
- Ebeling, H.; White, D. A.; Rangarajan, F. V. N. 2006, MNRAS, 368, 65
- Eyres, S. P. S., Bode, M. F., Skopal, A., Crocker, M. M.; Davis, R. J., Taylor, A. R., Teodorani, M., Errico, L., Vittone, A. A., Elkin, V. G. 2002, MNRAS, 335, 526
- Esch, D.N., Connors, A., Karovska, M., van Dyk, D.A., 2004, ApJ, 610, 1213
- Ezuka *et al.* 1998, ApJ, 499, 388
- Galloway, D.K. Sokoloski, J.L. 2004, ApJ Letters, 613, 61
- Hinkle, K.H. et al 1993, AJ, 105, 1074.
- Karovska, M., Carilli, C., and Mattei, J., 1998a, IAU Circ. No. 6970.
- Karovska, M., Carilli, C., and Mattei, J., 1998b, JASVO, 26, 97.
- Karovska, M. and Mattei, J., 1992, *JAAVSO*, **21**, 23
- Karovska, M., Schlegel, E., Hack, W., Raymond, J. C., & Wood, B. E. 2005, ApJ, 623, L137
- Karovska, M. 2003, Chandra Newsletter, Vol. 10, p.20-21
- Kellogg, E., Pedelty, J., and Lyon, R. 2001, ApJ, 563, L151.
- Leahy, D.A. & Taylor, A.R. 1987, AA, 176, 262
- Leahy, D.A. & Volk, 1957, ApJ, 440, 847
- Mikolajewska *et al.* 1998, *IAUCirc.* No. 6968
- Mukai, K., Ishida, M., Kilbourne, C., Mori, H., Terada, Y., Chan, K-W, 2006, PASJ, in press
- Park, S. *etb al.* 2002, ApJ, 567, 314
- Perryman *etb al.* 1997, A&A, 176, 262
- Rakowski, C.E. 2006, Ad. Sp. Res. 35, 6, 1017
- Raymond, J.C., Cox, D.P. & Smith, B.W. 1976, ApJ, 204, 290

- Skopal, A., Bode, M.F., Crocker, M.M., Drechsel, H., Eyres, S.P.S., Komzok, R. 2002, MNRAS, 335, 1109
- Sokoloski, J.L. and Kenyon, S. 2003, ApJ, 584, 1021)
- Stute, M. 2006, A&A, 450, 645
- Taylor, A.R., Seaquist, E.R., & Mattei, J.A. 1986, Nature, 319, 38
- Teranova, O.G., & Shenavrin, V. I. 2004, Astronomy Reports, 48, 813
- Weisskopf, M.C. *et al.* 2002, PASP, 114, 1
- Wheatley, P.J, & Kalmman T.R. 2006, MNRAS, 372, 1606
- Ybarra *et al.* 2006, astro-ph/0608162

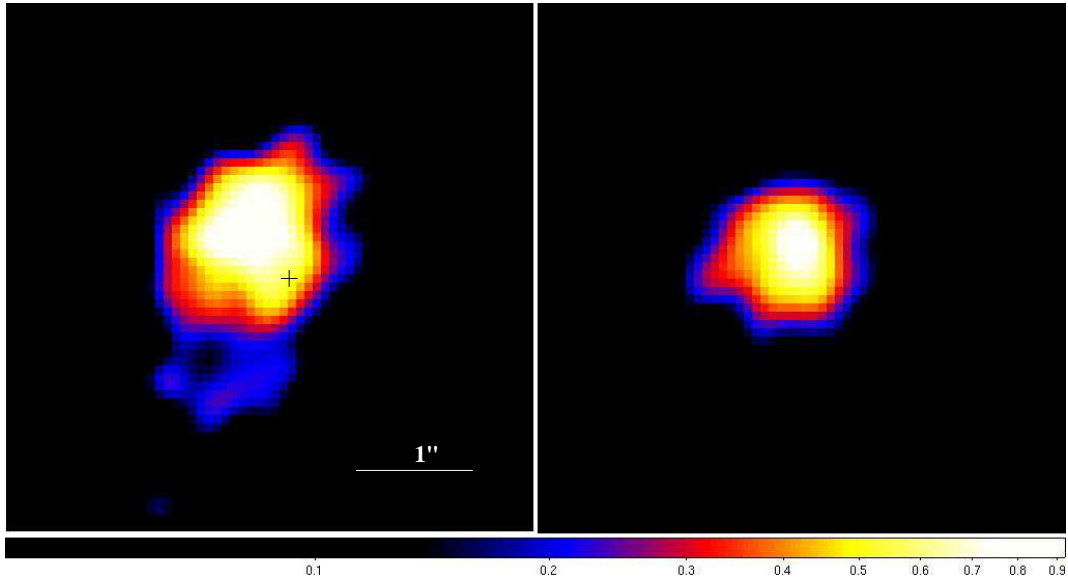


Fig. 1.— Adaptively smoothed ACIS-S images of CH Cyg in two spectral bands: left - soft band (0.2-2 keV) image, right - hard band (2-6 keV) image. North is up, East is to the left.

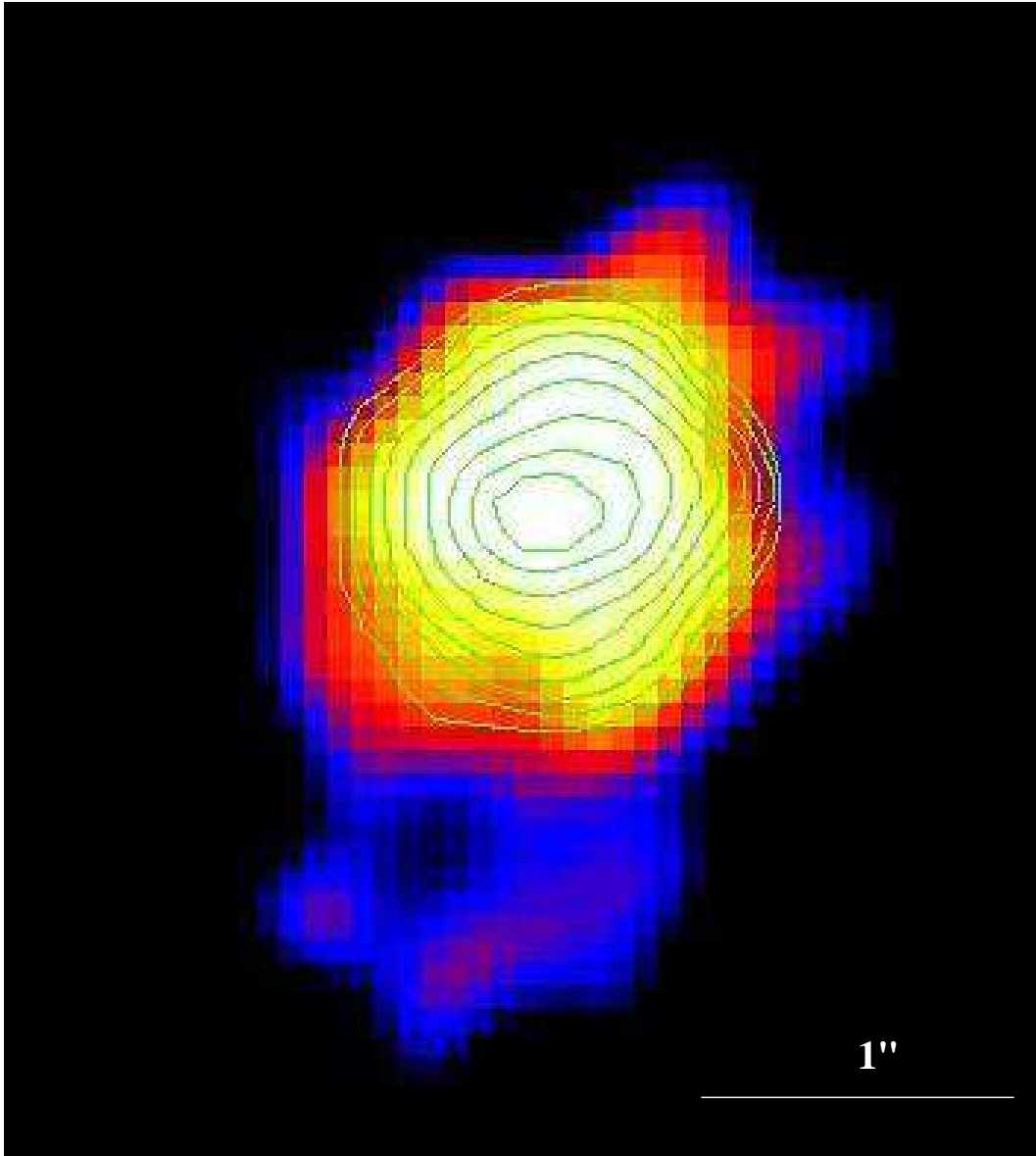


Fig. 2.— CH Cyg soft image with overlaid contours of the simulated PSF showing the loop at 1.5'' from the central source. The central source appears elongated in the N-W direction. North is up, East is to the left.

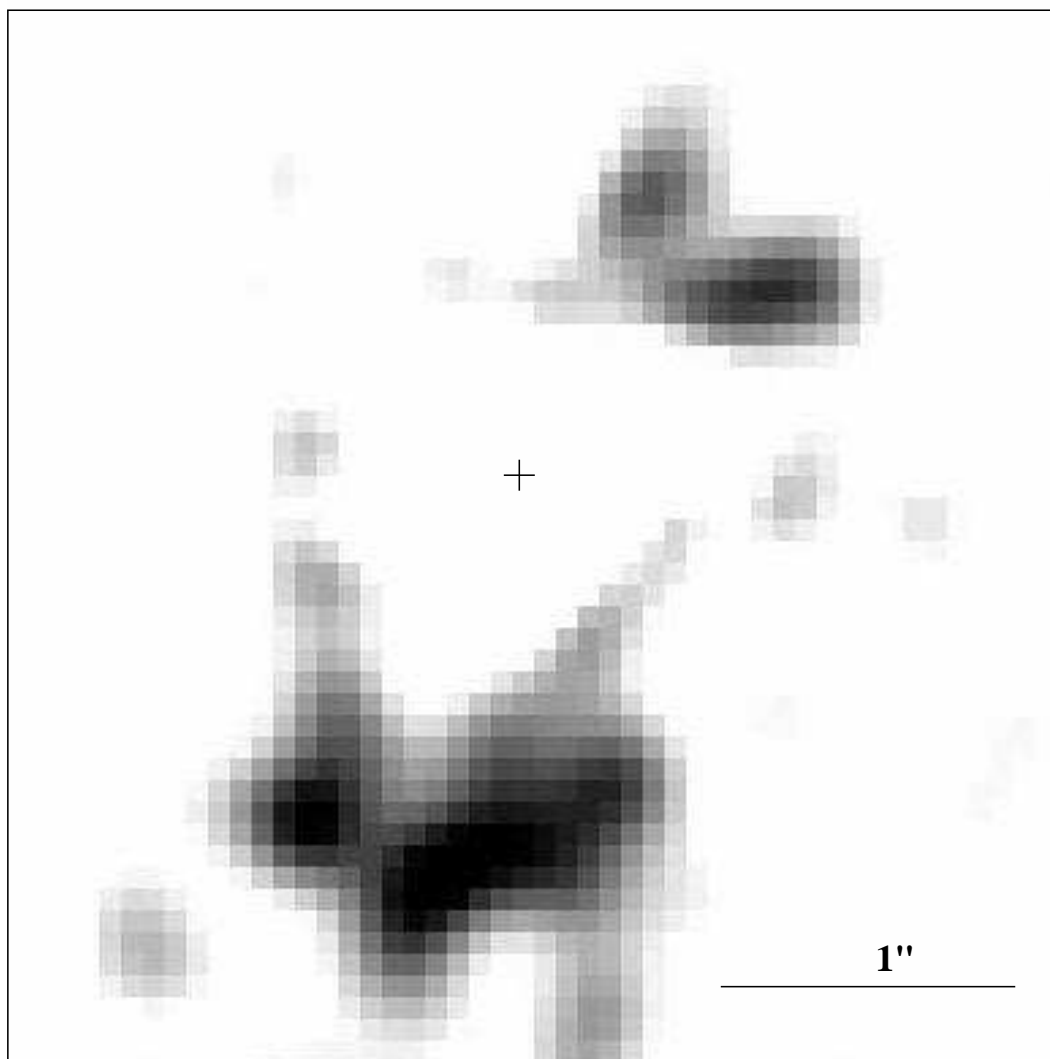


Fig. 3.— Soft image residuals after subtraction of the PSF show the loop-like structure to the south and extension toward the N-W at ~ 330 degrees

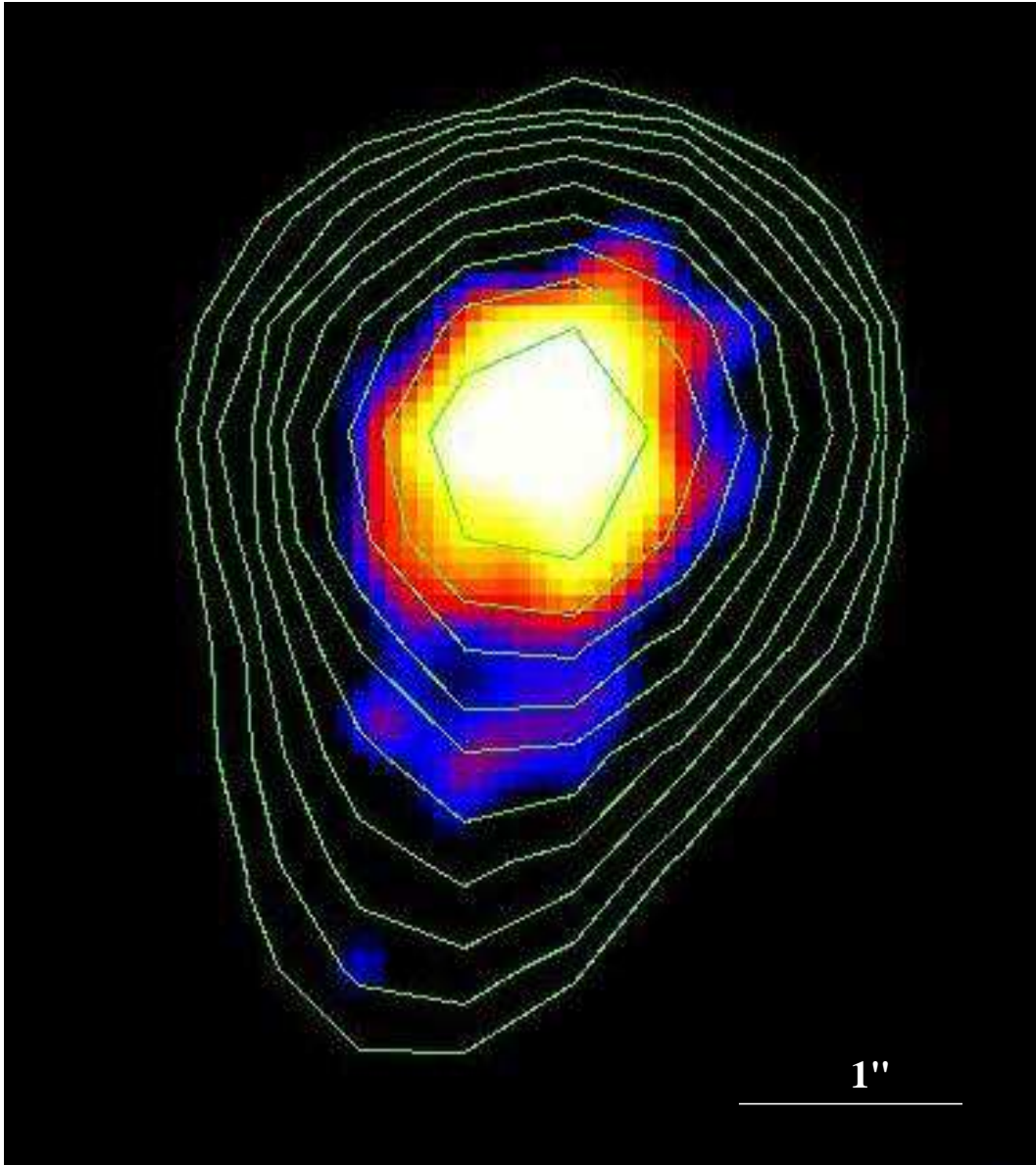


Fig. 4.— Comparison of the Chandra soft band adaptively smoothed image showing the central source and the loop with the Galloway and Sokoloski (2004) image (contours). The latter was smoothed using a gaussian with FWHM of $2''$.

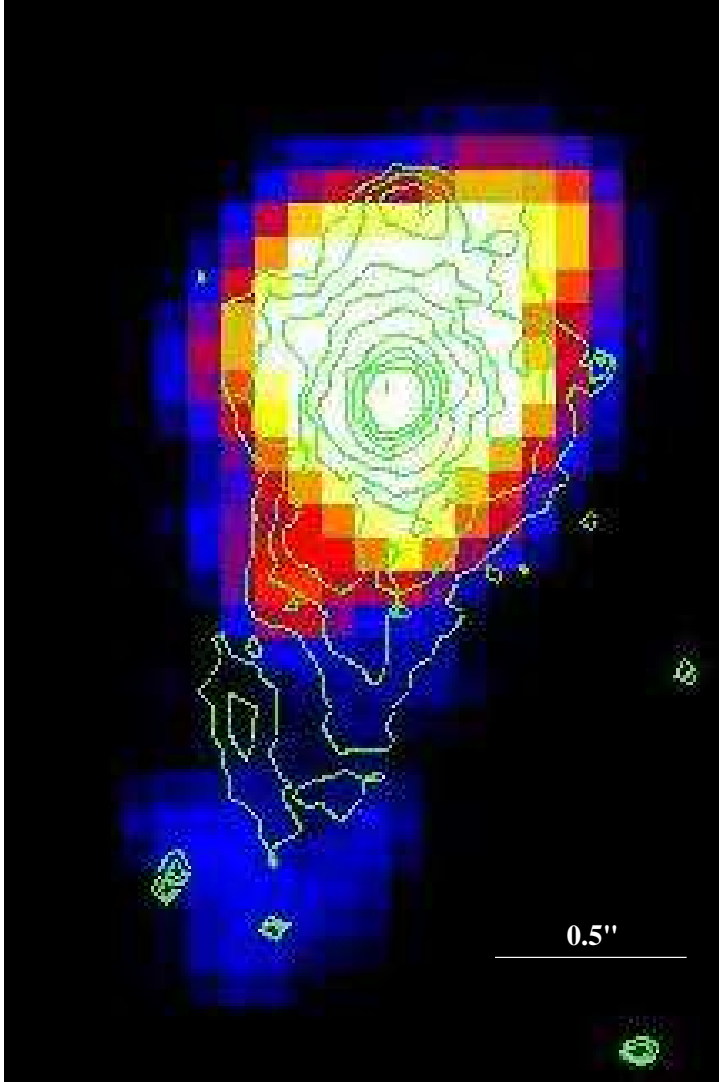


Fig. 5.— Chandra soft band image of CH Cyg deconvolved using simulated PSF. The image shows a complex multi-component structures similar to the structures detected in the adaptively smoothed image shown in Figure 2 but with improved resolution. In addition to the loop-like structure to the south of the central source, an elongated structure is detected at $\sim 0.7''$ from the central source in the direction of 330/150 degrees. Overlaid are contours of an OIII HST image obtained 1.6 years before the Chandra image showing similar morphology.

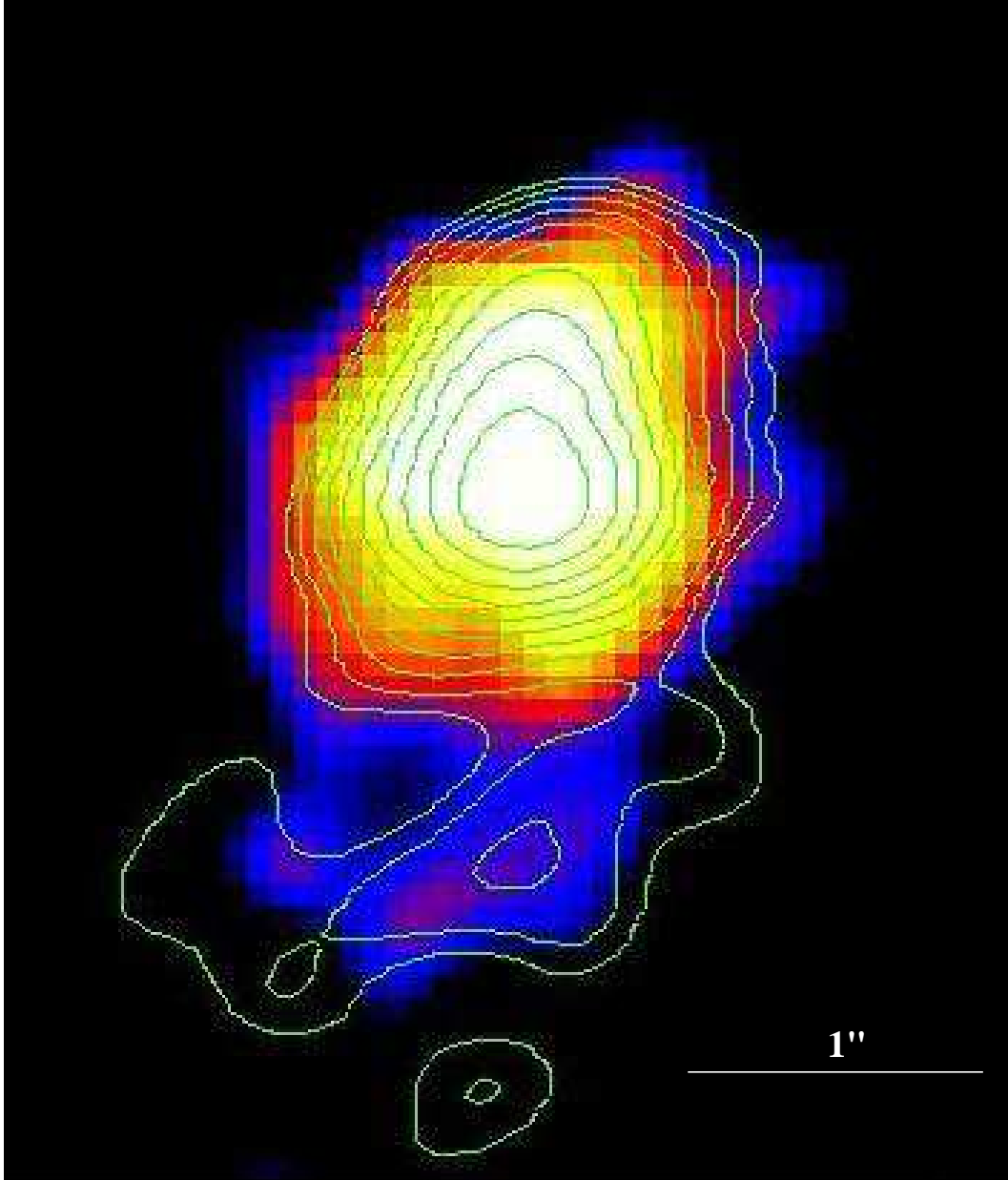


Fig. 6.— Overlay of 5GHz radio image contours on the soft X-ray smoothed image showing that the X-ray and radio loops are cospatial within the resolution of 0.3-0.4". The radio image was obtained 4.5 months before the Chandra image.